ACS APPLIED MATERIALS & INTERFACES

Research Article

www.acsami.org

Robust Superhydrophobic Silicon without a Low Surface-Energy Hydrophobic Coating

Sasha Hoshian,*[,†] Ville Jokinen,[†] Villeseveri Somerkivi,[†] Arcot R. Lokanathan,[‡] and Sami Franssila*[,†]

[†]Department of Materials Science and Engineering and [‡]Department of Pulp and Paper Technology, Aalto University School of Chemical Technology, 02150 Espoo, Finland

Supporting Information

ABSTRACT: Superhydrophobic surfaces without low surface-energy (hydrophobic) modification such as silanization or (fluoro)polymer coatings are crucial for water-repellent applications that need to survive under harsh UV or IR exposures and mechanical abrasion. In this work, robust low-hysteresis superhydrophobic surfaces are demonstrated using a novel hierarchical silicon structure without a low surface-energy coating. The proposed geometry produces superhydrophobicity out of silicon that is naturally hydrophilic. The structure is composed of collapsed silicon nanowires on top and bottom of T-shaped micropillars. Collapsed silicon nanowires cause superhydrophobicity due to nanoscale air pockets trapped below them. T-shaped micropillars significantly decrease the water contact angle hysteresis because microscale air pockets are trapped between them and can not easily escape. Robustness is studied under mechanical polishing, high-energy photoexposure, high temperature, high-pressure water shower, and different acidic and solvent environments. Mechanical abrasion damages the nanowires on top of micropillars, but those at the bottom survive. Small increase of hysteresis is seen, but the surface is still superhydrophobic after abrasion.

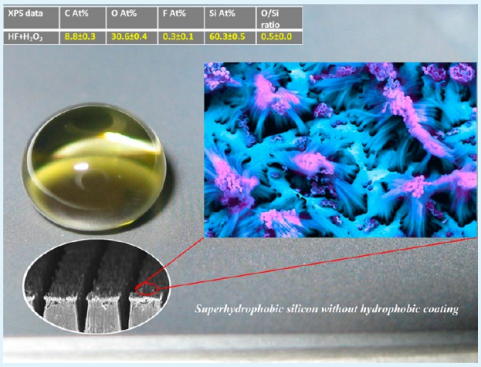

KEYWORDS: *water-repellent, robust, micro/nanoscale air pockets, hoodoos, etching, nanowire*

1. INTRODUCTION

Superhydrophobicity means high contact angle (>150°), low hysteresis (small difference in advancing and receding contact angles), and easy roll-off (a tilt angle of a few degrees).[1−9] It has been a very active research field recently due to its promise in a wide field of applications, including solar cells, sensing, self-cleaning, drug delivery, and microfluidic devices.[10−21]

Superhydrophobicity was inspired by the lotus effect, and its basic mechanism includes both the topography and the surface chemistry. There are two superhydrophobic states defined by contact angle hysteresis that is a difference between advancing and receding angles. One is a low hysteresis state (rolling state or "Cassie−Baxter" (CB) state), and the other is a high hysteresis state (sticky state or "Wenzel" state). The CB state is explained by trapped (hydrophobic) air between the microstructures. Water droplets remain almost spherical on both states, but they will easily roll off from CB surface even by a slight tilting of the surface, while they stick to the surface in Wenzel state.

Typically roll-off superhydrophobicity is achieved by separately making the topography single or dual (hierarchical) scale, followed by applying a low surface-energy coating on it. There are some examples of these low surface-energy materials reported in literature such as perfluorooctyl trichlorosilane (PFOS), 3,3,3-trifluoropropyl trichlorosilane (TFPS), dodecyl trichlorosilane (DTS), octadecyl trichlorosilane (ODTS), perfluorooctyl trichlorosilane (PFOS), and (fluoro)polymer (CHF_3 or C_4F_8).[17,20,22−28]

However, low surface-energy coatings cause problems in many practical applications due to the degradation of organic coating caused by mechanical wear, UV radiation, or abrasive particles. As an example, UV exposure is common in microfluidic devices to switch hydrophilic sites to be superhydrophilic, while superhydrophobic walls surround them.[29] Long-term exposures cause decomposition of coatings on superhydrophobic walls and liquid leaks through the walls. Additionally, the conformality of many coatings is not good enough to cover the nanostructures without changing the topography. Quite often the limiting factor for the use of superhydrophobic surfaces is the stability of the fluoropolymer, silane, or other coatings.

Some oxide nanowires (like zinc oxide), which are produced by chemical sintering methods, are also reported to be superhydrophobic without low surface-energy coatings, but they are not robust in high temperatures and during UV treatment; in fact they become hydrophilic after some minutes of UV exposure.[30−32]

Metal-assisted chemical etching (MaCE) is a process to create nanostructures of silicon. Many papers report super-

Received: October 31, 2014
Accepted: December 18, 2014
Published: December 18, 2014

 © 2014 American Chemical Society

DOI: 10.1021/am507584j
ACS Appl. Mater. Interfaces 2015, 7, 941−949

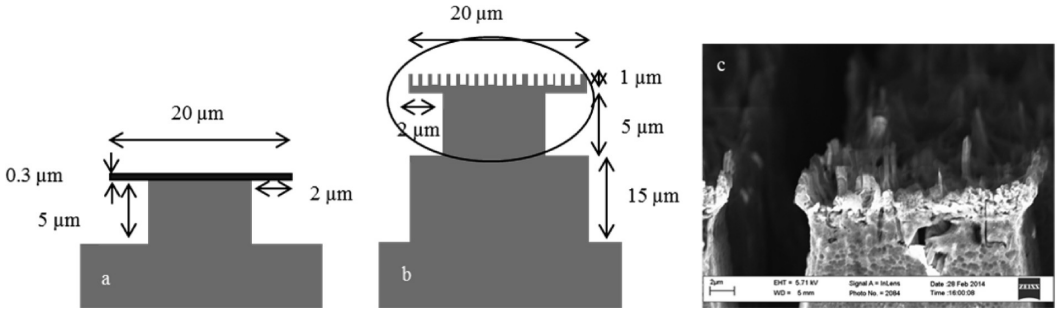

Figure 1. Side-view schematic of hoodoo structure. (a) Typical structure in literature with thin cap. (b) Our hierarchical structure. (c) SEM micrograph of nanowires on top of hoodoos.

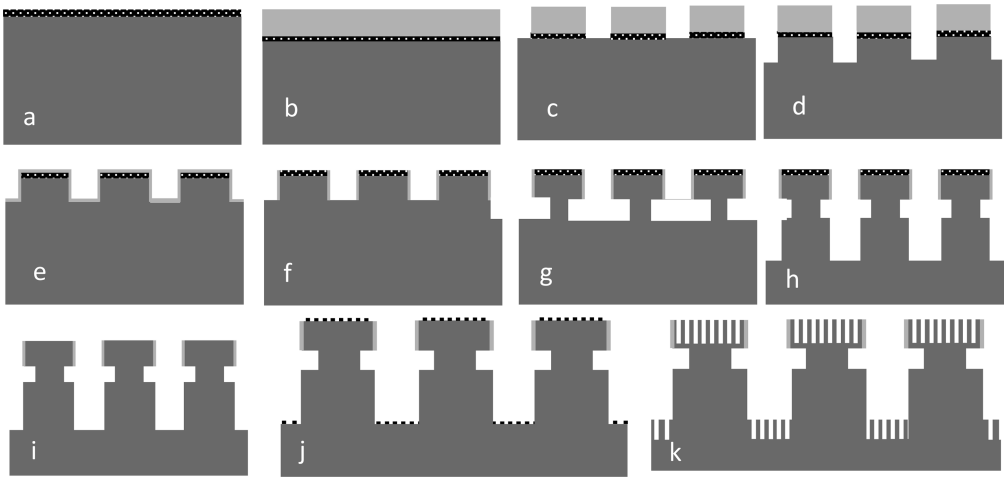

Figure 2. Schematic of fabrication process. (a) Al_2O_3 deposition on flat silicon wafer. (b) Photoresist spin-coated on Al_2O_3. (c) Photolithography to pattern Al_2O_3. (d) Anisotropic silicon etching. (e) Removing the photoresist and depositing TiO_2. (f) Anisotropic etching of TiO_2 in ICP resulting in protected sidewalls. (g) Isotropic etching of silicon to produce the neck of hoodoos. (h) Anisotropic etching of silicon to increase pillar height. (i) Wet etching of Al_2O_3. (j) Deposition of noncontinues Ti/Au thin film. (k) Metal-assisted etching of silicon in HF/H_2O_2 solution.

hydrophobicity of MaCE nanostructures, but low surface-energy chemical coating was needed to get superhydrophobic surfaces.[23,24,26,33−35] In MaCE, an aqueous solution containing hydrogen fluoride (HF) and an oxidant hydrogen peroxide (H_2O_2) etches silicon anisotropically when a thin layer of noble metal (e.g., Ag, Au, Pt) is used as a catalyst.[36] Noble metal acts as a cathode that is reduced in the solution and produces holes. These holes diffuse through the noble metal into silicon that is in contact with metal. Silicon is oxidized and dissolved by HF, forming nanopillars or pores.[37,38]

MaCE silicon structures have also been reported to show superhydrophobicity without polymer coatings.[22,39] In these papers either stability was not studied or it was reported to be inadequate, and low surface-energy coating was used eventually.[33] Turning intrinsically hydrophilic materials to superhydrophobic using single scale T-shape structures has been reported by other groups, but robustness was not reported.[40,41]

Here we report stable superhydrophobicity based on collapsed bushes of MaCE nanopillars on top and at the bottom of silicon T-shape micropillars (Figure 1). Importantly, a low surface-energy coating is not needed for superhydrophobicity. The superhydrophobicity is also robust against UV and IR exposure, chemical exposure, mechanical abrasion, water pressure, and high-temperature annealing. Main novelty is dual scale micro/nano overhangs with much-improved robustness. Micro-overhangs (T-shape micropillars) protect nano-overhangs (collapsed nanowires on the bottom) during mechanical abrasion. Also, dual scale micro/nano air pockets trapped below dual scale overhangs cause reduction of hysteresis dramatically.

2. EXPERIMENTAL SECTION

2.1. Fabrication of T-Shaped Silicon Micropillars (silicon thick-cap hoodoos). Our fabrication process is shown in Figure 2 (a−k). One-side polished p-type silicon wafer was used as substrate. Atomic layer deposition (ALD) of thin-layer aluminum oxide (Al_2O_3) 25 nm ± 1% thick at 300 °C was used as a mask during silicon etching (Figure 2a). Aluminum oxide layer was grown in a Beneq TFS-500 reactor using trimethylaluminum (TMA) as a metal precursor and water as a precursor for oxidation. The pressure in the reactor was 4 Torr. Nitrogen was used as a carrier gas and to purge reaction gases from the reactor during each reactin half cycle. 250 ms precursor pulses and 1 s purge pulses (the same for both precursors) were used. To pattern the aluminum oxide layer, 1.5 μm of AZ5214 photoresist was spin-coated on it (Figure 2b). Hexamethyl disilazane (HMDS) was used to improve the adhesion of photoresist to the substrate. After photolithography, aluminum oxide layer was wet-etched at 50 °C (Figure 2c). Etchant contained 80 wt % phosphoric acid, 5 wt % nitric acid, and the remaining 15 wt % was water. Patterns consisted of 20 μm squares with 5 μm spacing. After patterning the Al_2O_3 layer, silicon was anisotropically etched using inductively coupled plasma and deep reactive-ion etching (ICP-DRIE, Plasmalab System 100, Oxford Instruments) at −120 °C for 1 min to make the 1 μm thick cap (Figure 2d). All the ICP etching steps were done in 10 mTorr chamber pressure. A mixture of SF_6/O_2 was used as the anisotropic etching gas, and their flows were set to 40 sccm/6.5 sccm, while the

DOI: 10.1021/am507584j
ACS Appl. Mater. Interfaces 2015, 7, 941−949

Table 1. Water Contact Angle Measurements

Contact angle measurement	HF treated flat silicon before MaCE	flat silicon after MaCE (Fig 3d)	cylindrical pillars before MaCE	cylindrical pillars after MaCE (Fig 6)	micro-hoodoos before MaCE (Fig 3a)	micro-hoodoos after MaCE (Fig 3b)
Schematics	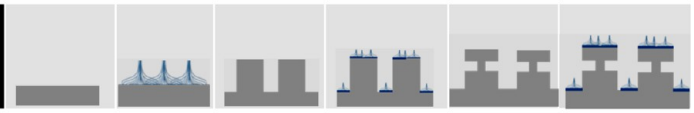					
Advancing	75±1°	154±2°	51±1°	160±1°	105±1°	168±1°
Receding	52±1°	132±2°	24±2°	142±1°	90±1°	166±2°
Hysteresis	23±1°	22±2°	27±2°	18±2°	15±1°	2±1°
Static	71±2°	152±1°	38±1°	155±1°	100±1°	165±2°
1 hour heating in 350°C	71±2°	152±1°	38±1°	155±2°	100±1°	165±1°
30 min UV exposure	71±2°	152±1°	38±1°	155±1°	100±1°	165±1°
Roll off angle for 4μl water droplet	sliding at 5 ±1°	20±1°	sticky	10±1°	sticky	4±1°
Advancing after abrasion	43±2°	51±1°	15±2°	152±1°	6±1°	160±1°
Receding after abrasion	21±2°	20±1°	5±1°	122±1°	~0°	135±1°
Hysteresis after abrasion	22±2°	31±1°	10±1°	30±1°	6±1°	25±1°
Static after abrasion	39±2°	50±1°	13±2°	145±1°	~0°	155±1°

powers of inductively and capacitively coupled power sources were 1000 and 2 W, respectively.

Then photoresist was removed in acetone, and 25 nm of titanium oxide (TiO_2) was deposited using the same ALD system for passivation of the surface (Figure 2e). Water and $TiCl_4$ were used as precursors for ALD of TiO_2. 250 ms precursor pulses and 250 ms purge pulses (the same for both precursors) were used. Mixture of SF_6 and oxygen (40 sccm/6.5 sccm) in ICP reactor was used to etch TiO_2 (Figure 2f). Next step is isotropic silicon etching, and it was done using SF_6 80 sccm without oxygen (Figure 2g). We did another anisotropic silicon etching step for 8 min to get 8 μm bodies of microhoodoos (Figure 2h). Then the resistive Al_2O_3 layer was etched using the same wet etching as explained (Figure 2i).

2.2. Collapsed Silicon Nanowires (nanobushes). Metal-assisted chemical etching (MaCE) was used to make the nanowires on top and bottom of hoodoos (Figure 2 j,k). We deposited 2 nm of Ti/5 nm of Au on our samples and on a reference sample using e-beam evaporation system (IM-9912 from Instrumentti Mattila Oy). The base pressure was 4×10^{-7} Torr at room temperature. Deposition rate was 1.2 Å/s for both materials as measured by quartz crystal microbalance. A solution of 1:1 HF (50%) and H_2O_2 (30%) was prepared for MaCE. We etched the samples for 10 s and then rinsed them with deionized water for 1 min and dried them immediately with N_2 blowing gun. The remaining gold was removed in aqua regia (1:3 volume mixture of 69% HNO_3 and 37% HCl) for 1 min at room temperature and 5 s dipping in solution of 1:1 HF (50%) and H_2O_2 (30%).

2.3. Sample Characterization. Advancing and receding contact angles were measured using the sessile droplet method (Theta, Biolin Scientific, Espoo, Finland). Results are averages of ten measurements.

XPS wide-scan spectra were recorded using a Kratos Axis $Ultra_{DLD}$ instrument (Kratos Ltd., Telford, U.K.) equipped with a monochromated aluminum anode (Al Kα 1486 eV) operating at 100 W (12.5 kV and 8 mA) with 160 eV of pass energy. A hybrid lens mode was employed during analysis (electrostatic and magnetic). Spectra were measured at three areas on each sample, and the value presented here corresponding to each sample is the average of three measurements. The photoelectron takeoff angle with respect to the normal to the surface in all measurements is 0°. The measured binding energy positions were charge corrected with reference to 285.0 eV, corresponding to the C−C/C−H species. The elemental peaks of the spectra were quantified using CasaXPS software.

A 1500 W infrared lamp (Infrared IC Heater T962) and a UV lamp 1300 W with 105 mW/cm^2 and 365 nm wavelength (ECE 2000 Modular DYMAX) was used for IR and UV exposure. We used a flat silicon wafer coated with 1*H*,1*H*,2*H*,2*H*-perfluorododecyltrichlorosilane (Sigma-Aldrich) for 2 h in gas phase in room temperature and atmospheric pressure, as reference sample to study the robustness of superhydrophobicity in IR and UV exposure. Heat treatment was done using PEO-601 furnace.

Mechanical stability of superhydrophobic samples was tested using a polyester/cellulose Technicloth II wipes (ITW Texwipe, TX 1112) for abrasion with pressure of 3.50 kPa.[24] The superhydrophobic surface was faced to the wipe paper and moved in one direction for 25 cm with speed of 60 mm/s in 4 s. Water contact angle and hysteresis measurements were carried out before and after abrasion test.

3. RESULTS AND DISCUSSION

3.1. Superhydrophobic Silicon Produced by MaCE. Advancing and receding contact angle measurements are collected in Table 1. It shows MaCE on flat silicon (reference sample) produces superhydrophobicity with 152° water contact angle and hysteresis is 22° although HF-treated flat silicon is

DOI: 10.1021/am507584j
ACS Appl. Mater. Interfaces 2015, 7, 941−949

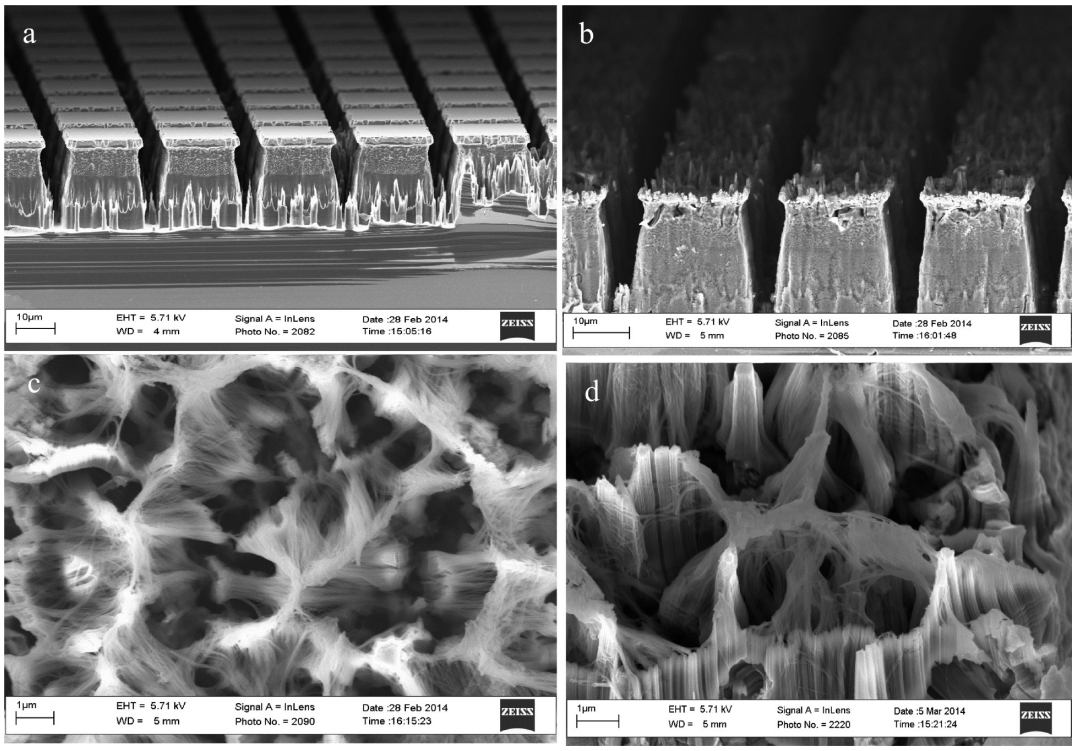

Figure 3. SEM micrograph of hoodoos after DRIE process and (a) before MaCE and (b) after MaCE. Top view high magnification of nanowire bushes (c) on top of a hoodoo after MaCE and (d) on flat silicon after MaCE.

hydrophilic before MaCE. Sliding angle for flat silicon samples after MaCE is ∼20°.

Only 10 s of MaCE is enough to get 1 μm of high silicon nanowires. We used a thin layer of evaporated gold as a catalyst. Titanium layer improved the adhesion of gold to silicon. Otherwise the gold layer would be peeled off immediately during the MaCE process. The islands of gold act as starting point for MaCE etching, resulting in vertical silicon wires. The key points are optimizing the noble metal thickness to get a large number of uniformly sized and uniformly distributed gold nanoislands on the silicon surface. We used 5 nm of Au with 2 nm of titanium adhesion layers. Thicker metal layer causes a uniform etching due to lack of nanoislands, which is not desired. Duration of etching is also important because long etching can cause destruction of the nanowires.

Collapse of silicon nanowires into nanobushes (Figure 3d) causes superhydrophobicity without low surface-energy coating. This is due to nanoscale air pockets that are captured and kept under collapsed nanowires. It is important to notice that aligned nanowires are not robustly superhydrophobic because air pockets can escape easily from them and because they need to have final low surface-energy modification to be superhydrophobic.[33]

High surface tension of water during the rinsing step after MaCE causes the nanowires to stick together and to collapse to nanobushes like those reported in ref 42. For robust superhydrophobicity, collapsed nanowires are desirable due to re-entrant structures that are necessary for making low contact fraction of solid−liquid, which are the main reason for superhydrophobicity without low surface-energy coatings.

Although MaCE on flat silicon produces superhydrophobic surfaces, the hysteresis of 22° is not low enough to result in a small sliding angle. On the other hand mechanical abrasion can easily destroy nanowires on the surface, and superhydrophobicity will be lost.

3.2. MaCE on Top and Bottom of T-shape Pillars. To improve the performance of the planar MaCE surface, we added a second roughness scale with T-shape micropillars to our nanostructures. If cap of T-shape pillars are made out of thick silicon, then MaCE can be done on top and bottom of them (Figure 3a,b).

Our T-shape micropillar fabrication technique is based on sidewall passivation by ALD of TiO_2. DRIE is anisotropic process that does not etch the thin film on the sidewall, but removes it from horizontal surfaces. T-shape cap thickness is simply determined by the duration of the first DRIE etch step. MaCE of the thick silicon cap makes the nanowire bushes. A highly regular array of T-shape micropillars with 20 μm diameter, 5 μm pitches, and 25 μm height was demonstrated in this work (Figure 3). But we are able to tune all the dimensions of the pillars: height, diameter, and spacing, cap thickness, and nanowire dimensions, too (bigger collapsed silicon nanowires are demonstrated in Supporting Information, Figure S2).

The first critical challenge is to make a thick cap for T-shape pillars to use it as a substrate in MaCE process. To do so, we need to consider two main points: (1) use a deposition method that is assuring good step coverage of the sidewalls, (2) use a material that is resistant in isotropic ICP-DRIE of silicon.

Atomic layer deposition of TiO_2 is the choice that meets both requirements. Step coverage of ALD is excellent, and ALD of TiO_2 protects the sidewalls of the cap of the T-shape pillars during isotropic etching. On the other hand, TiO_2 is etchable in a gas mixture of SF_6 and O_2 (anisotropic silicon etching in ICP-DRIE), while it is resistant to SF_6 during isotropic silicon etching. The etch rate of silicon is much higher than etch rate of TiO_2 using SF_6, so the oxide remains as protection of cap, while silicon is getting etched to form the overhanging

DOI: 10.1021/am507584j
ACS Appl. Mater. Interfaces 2015, 7, 941−949

structure. Final anisotropic silicon etching step was done to increase the amount of microscale air pockets to improve the robustness of T-shape pillars.

Comparing contact angle measurements (Table 1) of MaCE on flat silicon and on thick cap T-shape micropillars shows huge reduction of hysteresis (22° to 2°) on hierarchical T-shape structures, which confirms our hypothesis of embedding microscale air pockets between T-shape micropillars. Schematic of microscale air pockets captured between two superhydrophobic surfaces is illustrated in Figure 4.

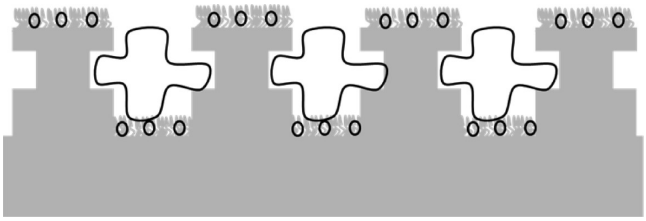

Figure 4. Schematic of hierarchical silicon structures. Nanoscale air pockets (○) trapped under collapsed nanowires on top and bottom of T-shape micropillars make dual-layer superhydrophobicity, while microscale air pockets (open +) sandwiched between micropillars significantly decrease the hysteresis.

Rolling state of hierarchical superhydrophobic samples is shown in Figure 5. A 4 μL water drop comes close to the surface, and it rolls off as soon as it is released from the needle. The rolling angle is less than 5°.

Tuteja introduced hoodoo (T-shape) structures;[43] overhanging shelves on top of micropillars (Figure 1a), but they used thin silicon dioxide as the cap of hoodoos to make overhanging structures. Since oxides are hydrophilic they need to be modified with a low surface-energy coating. Our structures (Figure 1b) consist of a thick silicon cap instead of thin oxides. Thick silicon cap on hoodoos is necessary otherwise MaCE can not be done on top of them.

To study the T-shape overhanging effect on hysteresis, we also studied the superhydrophobicity of samples with MaCE collapsed nanowires on top of cylindrical micropillars (without T-shape micro-overhanging effect) with 20 μm diameter, 5 μm pitches, and 25 μm height (Figure 6). They do not show low hysteresis superhydrophobicity. Static water contact angle of these samples is 155° with 18° hysteresis. It shows how microscale air pockets are critical for low hysteresis superhydrophobicity. Air pockets escape easily from cylindrical pillars. Water penetration between cylindrical pillars increases the hysteresis.

3.3. XPS Measurement. For better understanding the effect of MaCE process on surface chemistry, we prepared two samples: one dipped in HF (50%) and the other in HF/H_2O_2 (1:1). The elemental surface composition of samples was characterized using XPS, and the data are collected in Table 2.

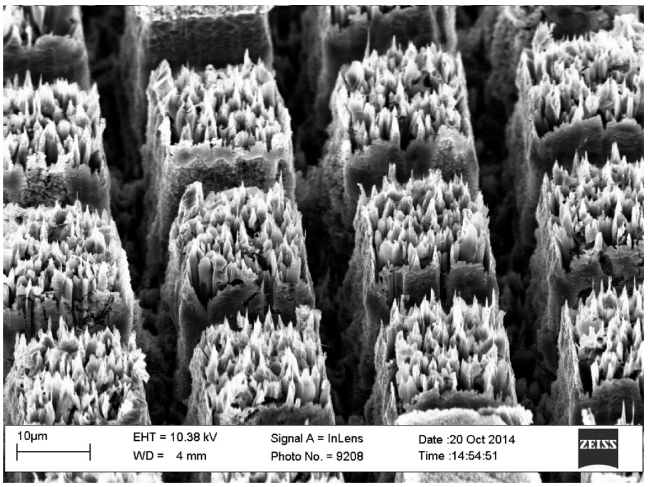

Figure 6. Nanostructures produced by MaCE on top and bottom of cylindrical micropillars.

The relative atomic percentage of fluorine was measured to be 0.2% ± 0.2% and 0.3% ± 0.1% for samples HF and HF + H_2O_2, respectively. This clearly shows that there is no significant change in the fluorine content during the surface treatment. Interestingly, there was at least a 2-fold difference in the value of O/Si ratio, 0.2 for HF sample, and 0.5 for HF/H_2O_2 sample. This increased O/Si ratio for HF/H_2O_2 sample suggests an elevated amount of oxidized silicon on the surface. Incorporation of O on the surface of HF/H_2O_2 sample also caused an increase in the value of relative atomic percentage of O, from 16.2% ± 0.4% for HF sample to 30.6% ± 0.4% for the sample corresponding to HF/H_2O_2. The carbon content of the surface remained unchanged, 8.9% ± 0.6% for HF sample and 8.8% ± 0.3% for HF/H_2O_2 sample, hence, showing that the changes in O/Si ratio and Si percentage are not due to any chemical modifications of surface-bound carbonaceous contaminants. Increasing the contact angle of flat silicon to 71 ± 2° after HF treatment (Table 1), compared to contact angle before treatment (36 ± 1°), is associated with Si−H and Si−CH_x groups on the surface[44] (hydrogen is not detectable on XPS, but 9% carbon was detected).

3.4. Study of Robustness. *3.4.1. UV and IR Exposure.* To show how our superhydrophobic samples are more robust than the ones with organic low surface-energy coatings, we exposed our samples with high-energy UV and IR lamps that are typically used for decomposition of organic molecules. Water contact angle measurements of our samples after 30 min of UV exposure are collected in Table 1. This time is usually enough to remove low surface-energy coatings such as organic materials from the surfaces.[45] Our samples, however, maintained the ultralow hysteresis superhydrophobic after 30 min of exposure. Because the superhydrophobicity depends on structure rather than surface chemistry, it is robust under UV exposure. We

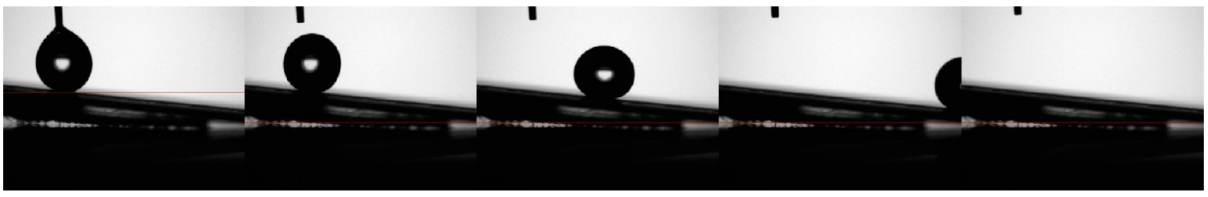

Figure 5. Rolling state for 4 μL water drop on hierarchical structures showing sliding angle <5°.

DOI: 10.1021/am507584j
ACS Appl. Mater. Interfaces 2015, 7, 941−949

Table 2. XPS Data

	C atom %	O atom %	F atom %	Si atom %	O/Si ratio
HF	8.9 ± 0.6	16.2 ± 0.4	0.2 ± 0.2	74.6 ± 0.8	0.2 ± 0.0
HF + H_2O_2	8.8 ± 0.3	30.6 ± 0.4	0.3 ± 0.1	60.3 ± 0.5	0.5 ± 0.0

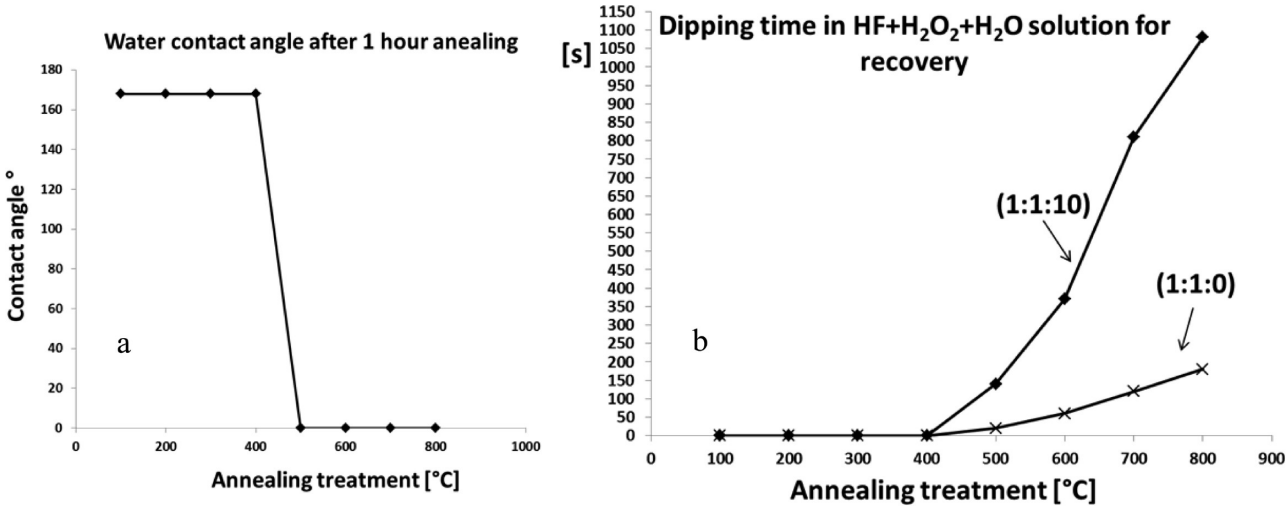

Figure 7. (a) Water contact angle after annealing treatment. (b) Recovery to superhydrophobic rolling state of samples after annealing by dipping them in $HF/H_2O_2/H_2O$ solution.

used a flat silicon wafer with a low surface-energy coating as reference sample. Water contact angle of reference sample before exposure was 125°, and it was reduced to 50° after 30 min of exposure due to decomposition of organic molecules from the surface. On the other hand, superhydrophobic TiO_2 or ZnO nanowires or nanoparticles become hydrophilic after 30 min of UV treatment.[30−32]

3.4.2. Thermal Annealing. The samples were annealed up to 800 °C to study the thermal stability of superhydrophobicity of the samples. Samples are superhydrophobic up to 400 °C.

Although superhydrophobicity was lost after 1 h at 450 °C, we discovered a very simple recovery process: by dipping the samples for a few seconds in HF/H_2O_2 (1:1) solution the original superhydrophobic surface was reconstructed. The changes in the water contact angle for annealed samples as a function of time and the dipping times for recovery to rolling superhydrophobic state (hysteresis <2°) are shown in Figure 7.

We explain the loss of superhydrophobicity by oxidation during annealing above 400 °C. Fast recovery is achieved due to oxide removal by 10 s of dipping time for the sample annealed for 1 h in 450 °C, and dipping time increased to 3 min for sample annealed at 800 °C. This fast recovery without any thin-film deposition is a big advantage of our work compared to low surface-energy coated superhydrophobic surfaces. Readers should be aware of dangers of HF processing. One can reduce the danger of HF by diluting the acid with water, but it increased the recovery time to minutes. A diluted solution of $HF/H_2O_2/H_2O$ (1:1:10) makes the recovery time to 60 s of dipping for the sample annealed for 1 h in 450 °C and 15 min for the sample annealed at 800 °C.

There is a limit for the number of recovery cycles due to etching the silicon in HF + H_2O_2 solution. We estimated 1000 recovery cycles to low hysteresis superhydrophobic state if every cycle takes 10 s. We considered the cap of hoodoos thickness of 1 μm and the etch rate of silicon in solution is 0.1 nm/s. Although the entire cap would have etched away after 1000 recovery cycles, surface would be superhydrophobic, but with higher hysteresis similar to cylindrical pillars with MaCE (Table 1).

3.4.3. Chemical Exposure. The chemical robustness of samples was studied by dipping them for 6 h in water, hydrofluoric acid (50%), acetic acid (99.8%), hydrochloric acid (37%), nitric acid (69%), acetone, isopropanol, and also hexane. Samples showed no change in contact angles in any of the cases.

3.4.4. Mechanical Abrasion. Table 1 shows that after abrasion our hierarchical samples remained superhydrophobic with contact angle of 155° and hysteresis of 25°. For better understanding the effect of our hierarchical structures on mechanical robustness, we did the same abrasion study on five other reference samples as mentioned in Table 1.

1. HF-treated flat silicon before MaCE: hydrophilic before abrasion with contact angle of 71° and became more hydrophilic with contact angle of 40° due to more roughening after abrasion.
2. Flat silicon after MaCE: superhydrophobic before abrasion with contact angle of 152° due to nanoscale overhangs but became hydrophilic with contact angle of 50°. Although abrasion adds some roughening to the surface, the nanoscale overhangs were destroyed, and surface was not hydrophobic any more.
3. Cylindrical pillars before MaCE: hydrophilic before abrasion and became more hydrophilic due to more roughening after abrasion.
4. Cylindrical pillars after MaCE: superhydrophobic with contact angle of 155° and hysteresis of 18° and became less hydrophobic with contact angle of 145° in sticky state with high hysteresis of 30° after abrasion. It means water droplet can easily penetrate through the cylindrical pillars after abrasion and stick to the surface due to destruction of nano-overhangs on top of pillars.

DOI: 10.1021/am507584j
ACS Appl. Mater. Interfaces 2015, 7, 941−949

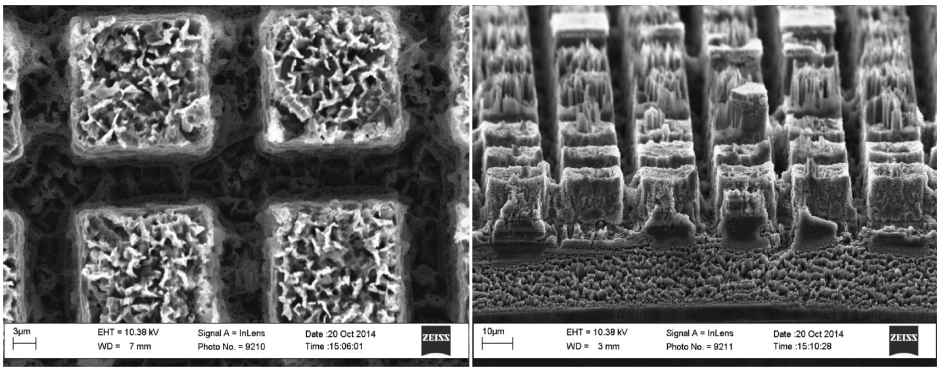

Figure 8. SEM micrograph of the sample after abrasion. (left) Microstructures act as sacrificial layer to survive the nanostructures at the bottom, and sample remained superhydrophobic. (right) Side-view of the same sample.

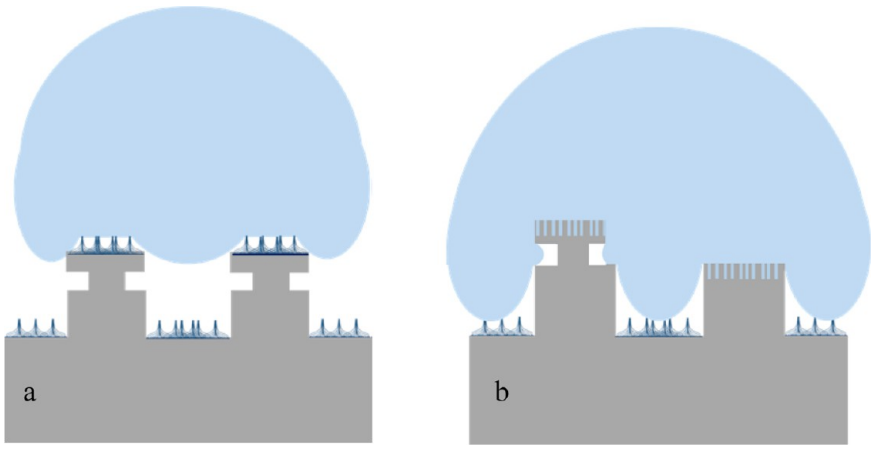

Figure 9. Schematic of water droplet on top of microhoodoos after MaCE. (a) Before abrasion droplet can not penetrate through, and hysteresis is very low. (b) Abrasion destroys MaCE nanostructures on top of pillars, but the surface still has considerably nanoscale roughness. Droplet semipenetrates through the micropillars and shows higher hysteresis but can not fully wet the bottom surface because of the MaCE nanowires protection, and the surface remained superhydrophobic.

5. Microhoodoos before MaCE: hydrophobic with contact angle of 100° with hysteresis of 15° and became superhydrophilic after abrasion. The hydrophobic state of microhoodoos before MaCE is specifically due to the trapped microscale air pockets below them; after roughening (abrasion) the overhangs are destroyed, and the air pockets can easily escape. Dual scale micro/nano roughening causes the superhydrophilicity of silicon.

For microhoodoos with MaCE, although micropillars are destroyed after abrasion, the bottom superhydrophobic layer plays a backup role and keeps the surface superhydrophobic, although with a higher hysteresis. Micropillars act as sacrificial layer during mechanical abrasion to improve survival of nanostructures at the bottom to keep the surface superhydrophobic.[46] We correlate the increase of hysteresis after abrasion to semipenetration of water droplet through micropillars. An SEM micrograph of destroyed micropillars after abrasion is shown in Figure 8. It shows how nanostructures at the bottom survive the abrasion. A schematic of water droplet on microhoodoos with MaCE before and after abrasion is illustrated in Figure 9. It shows a water droplet can semipenetrate through micropillars after abrasion but does not wet the bottom surface due to survival of MaCE nanostructures on the bottom. Surface remained superhydrophobic but with higher hysteresis compare to the surface before abrasion.

3.4.5. Water Pressure. We compare the robustness of our T-shape hierarchical samples with reference sample (MaCE on flat silicon) and also cylindrical hierarchical samples under water pressure. We dipped them for 5 cm under water. Our hierarchical sample superhydrophobicity was not changed after 6 h, and the contact angle was measured 165°. We also kept the T-shape sample with MaCE under tap water for 1 h, and it remained superhydrophobic without increasing the hysteresis. A movie of the same sample under tap water is available in Supporting Information. Both reference sample and cylindrical hierarchical sample become totally wet after 15 min with contact angle close to zero. Microscale air pockets escape easily from cylindrical micropillars. Water can penetrate through the cylindrical pillars after 15 min of dipping time and surface is not in rolling state superhydrophobic anymore.

Results show that T-shape micropillars are necessary for robust superhydrophobicity under water pressure. This is explained by microscale air pockets trapped below T-shape micropillars and can not easily escape from them.

4. CONCLUSIONS

We introduce a new method to fabricate robust low hysteresis superhydrophobic silicon surfaces without low surface-energy coatings. Decomposition of low surface-energy coatings in

DOI: 10.1021/am507584j
ACS Appl. Mater. Interfaces 2015, 7, 941−949

superhydrophobic surfaces is the main reason for avoiding them in long-term practical applications. Although HF-treated silicon is intrinsically hydrophilic (contact angle 71°), the proposed hierarchical structuring makes silicon superhydrophobic. We showed that structuring the surface can be dominant over the chemistry. Because the superhydrophobicity depends on structure rather than surface chemistry, it is robust under UV, IR, and chemical exposure, water pressure, and thermal treatments. It is also robust under mechanical abrasion due to existence of dual-layer structure.

About 10% of sunlight is in the UV range, and 95% of that can penetrate through the atmosphere. This is enough to reduce the robustness of superhydrophobicity based on organic low surface-energy coatings due to decomposition, over time. Our approach can improve the stability of superhydrophobic materials that are used in open environments such as self-cleaning buildings and cloths.

Chemically robust superhydrophobic surfaces have many applications in both research and industry. For example acidic rain causes loss of water-repelling properties of self-cleaning solar cells because of chemical reactions between organic coatings and acids.[47] Our approach can improve the efficiency of solar cells that are often located in industrial areas with high concentration of nitrogen oxide that produce nitric acid in acidic rains.

In fact these types of surfaces have a dual approach for their practical applications. On one hand they are very robust under harsh conditions below 400 °C. On the other hand they can be used in switching applications in higher temperature (>400 °C) environments where they become superhydrophilic.

The concept of embedding microscale air pockets in dual-layer superhydrophobic surfaces can be utilized in marine industry to reduce biofouling. For example the estimated costs due to fouling for the U.S. Navy fleet is between $180 M and $260 M per year.[48]

In future one can think of robust superhydrophobic surface in higher temperatures without low surface-energy coatings for heat-transfer systems. Recent studies revealed that superbiphilic (combination of superhydrophobic and superhydrophilic) surfaces are the most efficient surfaces for heat-transfer systems.[49] Our suggested surfaces have the ability to dramatically change the surface energy and can be used for heat-transfer systems involving superbiphilic approaches.

■ ASSOCIATED CONTENT

Supporting Information

Understanding of nanoscale air pockets trapped below collapsed silicon nanowires and also a movie of superhydrophobic sample under tap water. This material is available free of charge via the Internet at http://pubs.acs.org.

■ AUTHOR INFORMATION

Corresponding Authors

*E-mail: sasha.hoshian@aalto.fi. Phone: 003584603517. (S.H.)
*E-mail: sami.franssila@aalto.fi. (S.F.)

Author Contributions

The manuscript was written through contributions of all authors. All authors have given approval to the final version of the manuscript.

Notes

The authors declare no competing financial interest.

■ ACKNOWLEDGMENTS

This research was supported by the Academy of Finland (PROWET Project Nos. 263538 and 266820). Wafer processing took place at Aalto Nanofab cleanroom. The authors acknowledge A. S. Syed for his help in silicon etching process.

■ ABBREVIATIONS

ALD, atomic layer deposition
MaCE, metal-assisted chemical etching
ICP-DRIE, inductively coupled plasma−deep reactive ion etching

■ REFERENCES

(1) Crick, C. R.; Parkin, I. P. Preparation and Characterisation of Super-Hydrophobic Surfaces. *Chem.—Eur. J.* **2010**, *16*, 3568−3588.
(2) Verho, T.; Bower, C.; Andrew, P.; Franssila, S.; Ikkala, O.; Ras, R. H. A. Mechanically Durable Superhydrophobic Surfaces. *Adv. Mater.* **2011**, *23*, 673−678.
(3) Lafuma, A.; Quéré, D. Superhydrophobic States. *Nat. Mater.* **2003**, *2*, 457−460.
(4) Roach, P.; Shirtcliffe, N. J.; Newton, M. I. Progess In Superhydrophobic Surface Development. *Soft Matter* **2008**, *4*, 224−240.
(5) Yan, Y. Y.; Gao, N.; Barthlott, W. Mimicking Natural Superhydrophobic Surfaces and Grasping The Wetting Process: A Review On Recent Progress In Preparing Superhydrophobic Surfaces. *Adv. Colloid Interface Sci.* **2011**, *169*, 80−105.
(6) Guo, Z.; Liu, W.; Su, B.-L. Superhydrophobic Surfaces: From Natural To Biomimetic To Functional. *J. Colloid Interface Sci.* **2011**, *353*, 335−355.
(7) Ma, M.; Hill, R. M. Superhydrophobic Surfaces. *Curr. Opin. Colloid Interface Sci.* **2006**, *11*, 193−202.
(8) Li, X.-M.; Reinhoudt, D.; Crego-Calama, M. What Do We Need For a Superhydrophobic Surface? A Review On The Recent Progress In The Preparation Of Superhydrophobic Surfaces. *Chem. Soc. Rev.* **2007**, *36*, 1350−1368.
(9) Tian, Y.; Su, B.; Jiang, L. Interfacial Material System Exhibiting Superwettability. *Adv. Mater.* **2014**, *26*, 6872−6897.
(10) Leem, J. W.; Kim, S.; Lee, S. H.; Rogers, J. A.; Kim, E.; Yu, J. S. Efficiency Enhancement of Organic Solar Cells Using Hydrophobic Antireflective Inverted Moth-Eye Nanopatterned PDMS Films. *Adv. Energy Mater.* **2014**, *4*, 1301315.
(11) Smitha, V. S.; Jaimy, K. B.; Shajesh, P.; Jeena, J. K.; Warrier, K. G. UV Curable Hydrophobic Inorganic−Organic Hybrid Coating On Solar Cell Covers For Photocatalytic Self Cleaning Application. *J. Mater. Chem. A* **2013**, *1*, 12641−12649.
(12) Park, Y.-B.; Im, H.; Im, M.; Choi, Y.-K. Self-Cleaning Effect Of Highly Water-Repellent Microshell Structures For Solar Cell Applications. *J. Mater. Chem.* **2010**, *21*, 633−636.
(13) Kim, J.-Y.; Choi, K.; Moon, D.-I.; Ahn, J.-H.; Park, T. J.; Lee, S. Y.; Choi, Y.-K. Surface Engineering For Enhancement Of Sensitivity In an Underlap-FET Biosensor By Control Of Wettability. *Biosens. Bioelectron.* **2013**, *41*, 867−870.
(14) Anastasiadis, S. H. Development of Functional Polymer Surfaces with Controlled Wettability. *Langmuir* **2013**, *29*, 9277−9290.
(15) Yao, X.; Song, Y.; Jiang, L. Applications of Bio-Inspired Special Wettable Surfaces. *Adv. Mater.* **2011**, *23*, 719−734.
(16) Azarbayjani, A. F.; Lin, H.; Yap, C. W.; Chan, Y. W.; Chan, S. Y. Surface Tension and Wettability In Transdermal Delivery: A Study On The In-Vitro Permeation Of Haloperidol With Cyclodextrin Across Human Epidermis. *J. Pharm. Pharmacol.* **2010**, *62*, 770−778.
(17) Jokinen, V.; Kostiainen, R.; Sikanen, T. Multiphase Designer Droplets for Liquid-Liquid Extraction. *Adv. Mater.* **2012**, *24*, 6240−6243.

DOI: 10.1021/am507584j
ACS Appl. Mater. Interfaces 2015, 7, 941−949

(18) Almutairi, Z.; Ren, C. L.; Simon, L. Evaluation of Polydimethylsiloxane (PDMS) Surface Modification Approaches for Microfluidic Applications. *Colloids Surf., A* **2012**, *415*, 406−412.
(19) Feng, X. J.; Jiang, L. Design and Creation of Superwetting/Antiwetting Surfaces. *Adv. Mater.* **2006**, *18*, 3063−3078.
(20) Jokinen, V.; Sainiemi, L.; Franssila, S. Complex Droplets on Chemically Modified Silicon Nanograss. *Adv. Mater.* **2008**, *20*, 3453−3456.
(21) Sainiemi, L.; Jokinen, V.; Shah, A.; Shpak, M.; Aura, S.; Suvanto, P.; Franssila, S. Non-Reflecting Silicon and Polymer Surfaces by Plasma Etching and Replication. *Adv. Mater.* **2011**, *23*, 122−126.
(22) Cao, L.; Price, T. P.; Weiss, M.; Gao, D. Super Water- and Oil-Repellent Surfaces on Intrinsically Hydrophilic and Oleophilic Porous Silicon Films. *Langmuir* **2008**, *24*, 1640−1643.
(23) Xiu, Y.; Zhu, L.; Hess, D. W.; Wong, C. P. Hierarchical Silicon Etched Structures for Controlled Hydrophobicity/Superhydrophobicity. *Nano Lett.* **2007**, *7*, 3388−3393.
(24) Xiu, Y.; Liu, Y.; Hess, D. W.; Wong, C. P. Mechanically Robust Superhydrophobicity on Hierarchically Structured Si Surfaces. *Nanotechnology* **2010**, *21*, 155705.
(25) Song, Y.; Nair, R. P.; Zou, M.; Wang, Y. Superhydrophobic Surfaces Produced by Applying a Self-Assembled Monolayer to Silicon Micro/Nano-Textured Surfaces. *Nano Res.* **2009**, *2*, 143−150.
(26) Hu, H.; Swaminathan, V. V.; Farahani, M. R. Z.; Mensing, G.; Yeom, J.; Shannon, M. A.; Zhu, L. Hierarchically Structured Re-entrant Microstructures for Superhydrophobic Surfaces with Extremely Low Hysteresis. *J. Micromech. Microeng.* **2014**, *24*, 095023.
(27) Sun, G.; Gao, T.; Zhao, X.; Zhang, H. Fabrication of Micro/Nano Dual-Scale Structures by Improved Deep Reactive Ion Etching. *J. Micromech. Microeng.* **2010**, *20*, 075028.
(28) Qi, D.; Lu, N.; Xu, H.; Yang, B.; Huang, C.; Xu, M.; Gao, L.; Wang, Z.; Chi, L. Simple Approach to Wafer-Scale Self-Cleaning Antireflective Silicon Surfaces. *Langmuir* **2009**, *25*, 7769−7772.
(29) Zhang, X.; Zhang, J.; Ren, Z.; Zhang, X.; Tian, T.; Wang, Y.; Dong, F.; Yang, B. Photoinduced Cleaning of Water-Soluble Dyes on Patterned Superhydrophilic/Superhydrophobic Substrates. *Nanoscale* **2010**, *2*, 277−281.
(30) Gong, M.; Yang, Z.; Xu, X.; Jasion, D.; Mou, S.; Zhang, H.; Long, Y.; Ren, S. Superhydrophobicity of Hierarchical ZnO Nanowire Coatings. *J. Mater. Chem. A* **2014**, *2*, 6180−6184.
(31) Shaik, U. P.; Kshirsagar, S.; Krishna, M. G.; Tewari, S. P.; Dhar Purkayastha, D.; Madhurima, V. Growth of Superhydrophobic Zinc Oxide Nanowire Thin Films. *Mater. Lett.* **2012**, *75*, 51−53.
(32) Yao, L.; Zheng, M.; Li, C.; Ma, L.; Shen, W. Facile Synthesis of Superhydrophobic Surface of ZnO Nanoflakes: Chemical Coating and UV-Induced Wettability Conversion. *Nanoscale Res. Lett.* **2012**, *7*, 216.
(33) He, Y.; Jiang, C.; Yin, H.; Chen, J.; Yuan, W. Superhydrophobic Silicon Surfaces with Micro−Nano Hierarchical Structures Via Deep Reactive Ion Etching and Galvanic Etching. *J. Colloid Interface Sci.* **2011**, *364*, 219−229.
(34) Xiu, Y.; Zhang, S.; Yelundur, V.; Rohatgi, A.; Hess, D. W.; Wong, C. P. Superhydrophobic and Low Light Reflectivity Silicon Surfaces Fabricated by Hierarchical Etching. *Langmuir* **2008**, *24*, 10421−10426.
(35) Lee, C.; Kim, C.-J. Maximizing the Giant Liquid Slip on Superhydrophobic Microstructures by Nanostructuring Their Sidewalls. *Langmuir* **2009**, *25*, 12812−12818.
(36) Kim, J.; Kim, Y. H.; Choi, S.-H.; Lee, W. Curved Silicon Nanowires with Ribbon-like Cross Sections by Metal-Assisted Chemical Etching. *ACS Nano* **2011**, *5*, 5242−5248.
(37) Hildreth, O. J.; Brown, D.; Wong, C. P. 3D Out-of-Plane Rotational Etching with Pinned Catalysts in Metal-Assisted Chemical Etching of Silicon. *Adv. Funct. Mater.* **2011**, *21*, 3119−3128.
(38) Huang, Z.; Geyer, N.; Werner, P.; de Boor, J.; Gösele, U. Metal-Assisted Chemical Etching of Silicon: A Review. *Adv. Mater.* **2011**, *23*, 285−308.
(39) He, Y.; Jiang, C.; Yin, H.; Yuan, W. Tailoring the Wettability of Patterned Silicon Surfaces with Dual-Scale Pillars: From Hydrophilicity to Superhydrophobicity. *Appl. Surf. Sci.* **2011**, *257*, 7689−7692.
(40) Wang, J.; Liu, F.; Chen, H.; Chen, D. Superhydrophobic Behavior Achieved From Hydrophilic Surfaces. *Appl. Phys. Lett.* **2009**, *95*, 084104.
(41) Liu, T.; Kim, C.-J. Turning a Surface Superrepellent Even to Completely Wetting Liquids. *Science* **2014**, *346*, 1096−1100.
(42) Zhang, S.; Wang, X.; Liu, H.; Shen, W. Controllable Light-Induced Conic Structures in Silicon Nanowire Arrays by Metal-Assisted Chemical Etching. *Nanotechnology* **2014**, *25*, 025602.
(43) Tuteja, A.; Choi, W.; Mabry, J. M.; McKinley, G. H.; Cohen, R. E. Robust Omniphobic Surfaces. *Proc. Natl. Acad. Sci. U. S. A.* **2008**.
(44) Grundner, M.; Jacob, H. Investigations on Hydrophilic and Hydrophobic Silicon (100) Wafer Surfaces by X-ray Photoelectron and High-Resolution Electron Energy Loss-Spectroscopy. *Appl. Phys. A: Solids Surf.* **1986**, *39*, 73−82.
(45) Balaur, E.; Macak, J. M.; Taveira, L.; Schmuki, P. Tailoring The Wettability of TiO2 Nanotube Layers. *Electrochem. Commun.* **2005**, *7*, 1066−1070.
(46) Kondrashov, V.; Rühe, J. Microcones and Nanograss: Toward Mechanically Robust Superhydrophobic Surfaces. *Langmuir* **2014**, *30*, 4342−4350.
(47) Fernández-García, A.; Díaz-Franco, R.; Martinez, L.; Wette, J. Study of the Effect of Acid Atmospheres in Solar Reflectors Durability under Accelerated Aging Conditions. *Energy Procedia* **2014**, *49*, 1682−1691.
(48) Kirschner, C. M.; Brennan, A. B. Bio-Inspired Antifouling Strategies. *Annu. Rev. Mater. Res.* **2012**, *42*, 211−229.
(49) Betz, A. R.; Jenkins, J.; Kim, C.-J.; Attinger, D. Boiling Heat Transfer on Superhydrophilic, Superhydrophobic, and Superbiphilic Surfaces. *Int. J. Heat Mass Transfer* **2013**, *57*, 733−741.

DOI: 10.1021/am507584j
ACS Appl. Mater. Interfaces 2015, 7, 941−949